Climate Change Impacts on U.S. Electricity Demand: Insights from Micro-Consistent Aggregation of a Structural Model

Bentley Coffey*[1], Ari Stern[2], and Ian Sue Wing[2]

[1]Dept. of Economics, University of South Carolina
[2]Dept. of Earth & Environment, Boston University

January 30, 2015

Abstract

We use a large dataset of 2.3 million hourly observations of load across three regional power grids to estimate the effects of weather on the demand for electric power, and use the results to draw implications for the impacts of climate change. In a novel approach, we develop a micro-founded model of individual electricity demand for space conditioning that is rooted in the thermodynamics of building energy transfer, and demonstrate how it can be aggregated up to the weather zones that constitute the smallest geographic unit within regional power pools. What results is a deceptively simple reduced-form specification that can be estimated using standard panel data econometric techniques. Compared with existing semiparametric approaches in the empirical climate economics literature, our model generates marginal effects of heat on electricity demand which are smaller at moderate temperatures but substantially larger at the extreme temperatures. The difficulties faced by semiparametric approaches in capturing such tail impacts suggest that they may underestimate the increase in demand for peak power from climate-driven heatwaves, and with this, the generation and transmission investments necessary to ensure adequate electricity supply.

*

1 Introduction

Weather affects a remarkably broad swath of human activities. Concern over the potential impacts of future changes in the climate has led to a rapid emergence of a sizeable empirical literature documenting the influence of various meteorological variables—principally temperature—on a variety of economic outcomes (Dell et al, 2014b).

Electric power is one sector of the economy which is thought to be particularly exposed to meteorological shifts associated with climate change, because of the risk posed by extreme events (e.g., hurricanes) to electricity generation and distribution infrastructure on the supply side, and, in particular, changes in demand for heating and cooling services on the demand side. Cooling is especially important. Apart from temperate regions in western states, air conditioning (AC) is pervasive in U.S. households, with the installed base increasing from 68% of occupied housing units in 1993 to 87% in 2009 (EIA, 2009).[1] Moreover, together, heating and cooling account for almost half of household electricity use, and while AC's share of total consumption is small it has continued to increase steadily (EIA, 2009).[2] Since the late 1970s average U.S. temperatures have risen 0.31-0.48°F per decade, a trend which is expected to continue as the climate changes. Coincident net residential electricity use is expected to grow, with increased electricity demands for cooling outstripping savings from lower electricity demands due to reduced need for heating (Dell et al, 2014a).

While the pace at which *total* demand for electric power is projected to increase with climate warming is interesting, it is by no means the most important question to electric utilities, transmission companies and operators of electricity grids. These entities must plan and incur the costs of investments to satisfy the electric power system's *maximum* load, often years in advance of such peak demand being actually realized. Peak demand routinely occurs during the very hottest hours of the year, when a substantial fraction of the electricity supply is being for AC.[3] During these peri-

[1] `http://www.eia.gov/consumption/residential/reports/2009/air-conditioning.cfm`

[2] `http://www.eia.gov/todayinenergy/detail.cfm?id=10271`

[3] Simulation results for Phoenix suggest that AC usage accounted for 53% of total electricity demand and 65% of peak demand on extreme warm days (Salamanca et al, 2013). Estimates for Madrid in 2008 indicate that that while AC's share of load was only 6.7% over the entire cooling season, it was 20-33% of the July 19 peak (Izquierdo et al, 2011).

ods, the cost of operating the electricity generation units that supply peak power can be a factor of six times higher than average, with the result that a disproportionate fraction of annual electricity expenditures comes from the extreme temperature hours where cooling loads are at their maximum (see, e.g., Monitoring Analytics, 2013; Allcott, 2013). Recent findings that anthropogenic climate warming has a large and positive impact on the likelihood of heat waves—and temperature extremes more generally (Kharin et al, 2013; Peterson et al, 2013; Herring et al, 2014; Kodra and Ganguly, 2014), suggest that summer maximum temperatures to which transmission and generation capacity must be sized are likely to increase at least as rapidly as average temperatures. The central question, then, is how strongly *instantaneous* AC-driven demand is likely to respond to heatwaves that portend increasing extreme summer temperatures—whose duration can be as brief as a few hours.

Almost without exception, previous empirical papers identify the marginal impact on demand of additional time exposure to high temperatures from covariation between weather and energy use over time periods which are long compared to the peak—e.g., the effect of average daily temperature on annual residential energy consumption (Deschenes and Greenstone, 2011), or monthly electricity use (Aroonruengsawat and Auffhammer, 2011; Auffhammer and Aroonruengsawat, 2011). The key implication is that such low temporal resolution independent variables yield estimates that cannot be validly employed to make inferences about temperature impacts at hourly time scales. Moreover, even with time-averaged temperature measurements such as daily means, the paucity of observations in extreme high temperature bins ($> 90°$F, say) reduces the precision of the corresponding marginal effects. Finally, a key characteristic of the customary reduced-form approach is it estimates a constant marginal effect of additional time spent in intervals of temperature. But this formulation can run into problems in the semi-open tail intervals, where the implication is that an additional extreme day averaging 90°F will have the same effect as a day averaging 95°F—which belies the fact that hottest hour of extreme days can increase nonlinearly as daily average temperature increases.

In this paper we investigate the impact of temperature extremes on the peak demand for electricity by developing a novel thermodynamically micro-founded model of electricity demand

Figure 1: Independent System Operators Analyzed in this Study

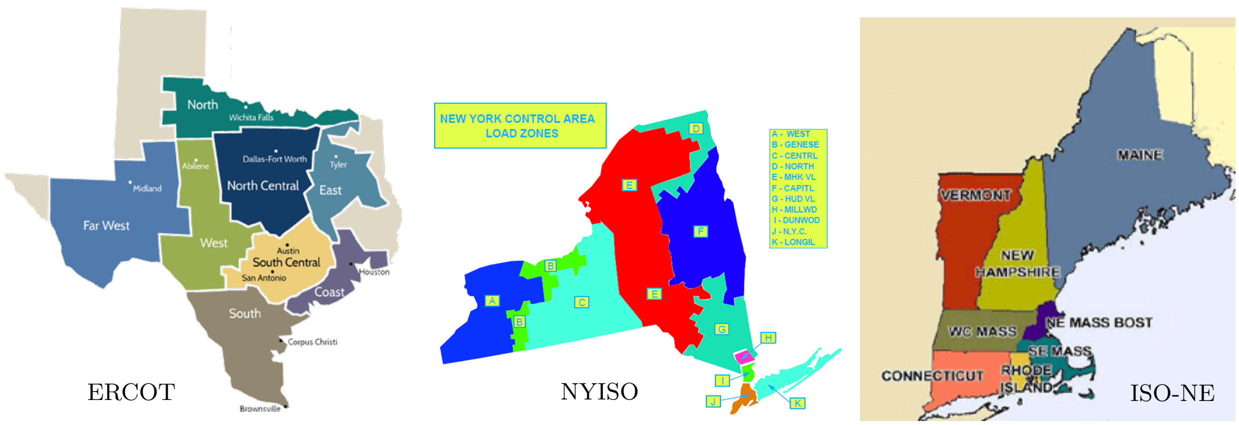

and estimating it on a unique high-frequency dataset, consisting of 2.3 million observations of hourly electric load over the period 2001-2012 for three power pools that account for 17% of U.S. electricity consumption. We estimate per capita demand for electricity as a function of temperature and humidity within "weather" zones of service territories of three ISOs: the Electric Reliability Council of Texas (ERCOT, which governs most of the state of Texas), New York ISO (NYISO, which governs the state of New York) and ISO New England (ISO-NE, which governs Connecticut, Maine, Massachusetts, New Hampshire, Rhode Island, Vermont). See Figure 1. Compared to existing empirical approaches, our model generates marginal effects of heat on electricity demand which are smaller at moderate temperatures but substantially larger at the extreme temperatures. suggesting that demand-side impacts in the literature .

The rest of the paper is organized as follows. In section 2 we develop a model of individual demand for electricity with non-discretionary consumption for heating, cooling and ventilation that is rooted in the thermodynamics of building energy transfer. Then, in section 3 we consistently aggregate this model up to the level of weather zones. Section 4 describes our data and briefly summarizes our estimation technique. Results are presented in section . Section 6 offers a summary and concluding remarks.

2 A Microfounded Thermodynamic Model

We assume that individual i's demand for electricity, q_i, follows Stone-Geary preferences. There is a "necessary" baseline quantity of electricity consumed for HVAC, w_i, which depends on weather; discretionary electricity demand over and above that level takes the familiar Cobb-Douglas form, and is financed out of disposable income remaining after covering all other necessary goods, g:

$$q_i = \gamma_i + w_i + \frac{\sigma}{p_E}\left(\mathscr{I}_i - p_E\left(\vartheta_i + w_i\right) - \sum_{g \neq E} p_g y_g\right) \tag{1}$$

where $\mathscr{I}$ is total income, σ is discretionary electricity's share of disposable income, p_E and p_g are prices of electricity and other goods, and y_g are the quantities of necessary consumption.

Our principal task is to develop a micro-founded model of electricity consumption for HVAC. Our key assumption is that individuals have identical preferences for thermal comfort, given by an ideal temperature (T^*) and humidity (H^*). To maintain environmental equilibrium at (T^*, H^*) climate control systems in the buildings where individuals spend time transfer enthalpy (e)—the sum of sensible heat and latent heat associated with phase changes in moisture—gained during each hour. Enthalphy gain/loss has four components: conduction, convection, radiation, and internal (e.g., heat released by the human body and electrical appliances).

For simplicity we assume that internal enthalphy is a constant ($\dot{e}_i^{\text{Internal}} = \iota$). Typical HVAC engineering calculations assume that internal enthalpy is just enough heat to raise the indoor temperature from standard room temperature (71 °F) by 6°F. Consequently, the customary setpoint in such calculations is 71°F but heating and cooling degree days are computed from a critical threshold of 65°F.

Fourier's Law models conduction (which only transmits heat) as linear in the internal-external differential between i's ideal temperature and the ambient temperature at her location, T_i:

$$\dot{e}_i^{\text{Conduction}} = \kappa_i^{\text{Conduction}}\left(T_i - T^*\right) \tag{2}$$

where κ is the ratio of building surface area to thermal resistance. Likewise, by Newton's Law, convection transmits both sensible and latent heat via air movement through ducts and open doors and windows according to the indoor-outdoor differentials in both temperature and ambient humidity H_i:

$$\dot{e}_i^{\text{Convection}} = \kappa_i^{\text{Convection}} \left[\underbrace{\chi_{pa}(T_i - T^*)}_{\text{Sensible Heat}} + \underbrace{\chi_{ev}(H_i - H^*) + \chi_{pv}(T_i \; H_i - T^* H^*)}_{\text{Latent Heat}} \right] \tag{3}$$

where χ_{pa} and χ_{pv} denote specific heat capacities of dry air (≈ 1.006 kJ kg^{-1}) and water vapor (≈ 1.84 kJ kg^{-1}) and χ_{ve} is the evaporation heat of water (≈ 2501 kJ/kg). Note that $\dot{e}_i^{\text{Conduction}}$ and $\dot{e}_i^{\text{Convection}}$ are both negative when the outdoor temperature is beneath the indoor temperature, a sign convention which indicates that heat is being lost.

Radiation is the conduit of energy gain from the sun, and as such must be accounted for with care. It is complicated by locations' dependence on insolation, which is governed by several physical processes: the Earth's axial tilt and its precession, the eccentricity of Earth's orbit, the specific location on Earth's surface, (absolute) solar time, and atmospheric conditions. For tractability we employ a reduced-form clear-sky approximation which uses four variables (time of day, day of year, latitude and longitude). Our method assumes that the sun's heat output is constant in all directions (following the Stefan-Boltzmann law for radiating bodies as a function of temperature), which means that at locations on the Earth's surface that are more distant from the sun incident radiation becomes more diffuse as the constant energy flux is spread across a larger spherical area:

$$\dot{e}_i^{\text{Radiation}} \propto \kappa_i^{\text{Radiation}} \cdot \Psi[x_i, y_i, t^{\text{Clock}}, d] \tag{4}$$

where (x_i, y_i) are the individual's grid coordinates, t^{Clock} is the wall-clock time at each location, and d is the day in the Julian calendar year. The heart of the approximation is the insolation function, Ψ, whose empirical elaboration is given in the appendix.

The enthalpy that must be transferred by HVAC systems depends on the temperature ranges governed by the HVAC mode: heating (H), ventilation (V), and cooling (C), which we denote using the index m. The enthalpy that must be transferred is given by:

$$\dot{e}_{i,m} = \begin{cases} -(\dot{e}_i^{\text{Conduction}} + \dot{e}_i^{\text{Convection}} + \dot{e}_i^{\text{Radiation}} + \dot{e}_i^{\text{Internal}}) & T_i \in (-\infty, T^* - \mathcal{O}] \quad m = H \\ \dot{e}_i^{\text{Conduction}} + \dot{e}_i^{\text{Convection}} + \dot{e}_i^{\text{Radiation}} + \dot{e}_i^{\text{Internal}} & T_i \in (T^* - \mathcal{O}, T^*) \quad m = V \\ \dot{e}_i^{\text{Conduction}} + \dot{e}_i^{\text{Convection}} + \dot{e}_i^{\text{Radiation}} + \dot{e}_i^{\text{Internal}} & T_i \in [T^*, +\infty) \quad m = C \end{cases} \tag{5}$$

where $\mathcal{O}$ is the temperature offset due to internal enthalpy. Recall that both $\dot{e}_i^{\text{Conduction}}$ and $\dot{e}_i^{\text{Convection}}$ are negative in heating or ventilation mode (when $T_i < T^*$). Hence, because both radiation and internal energy raise the indoor temperature, they reduce the climate control system's workload when in heating mode; likewise, because conduction and convection lower the indoor temperature when in the ventilation range, they reduce the climate control systems workload when in ventilation mode. Indeed, ventilation is the special temperature range that occurs when the internal energy is enough to put the indoor temperature over the ideal to trigger a need for cooling which can largely be mitigating via conduction and convection from cooler air outside (which can be increased by opening windows).

The electricity necessary to perform this work is determined by the coefficient of performance (CoP_m), the quantity of enthalpy transfer provided under heating, ventilation or cooling per unit electrical energy consumed. By the laws of thermodynamics this is bounded to some fraction, η_i, of the Carnot limit:

$$w_{i,m} = \frac{\dot{e}_{i,m}}{CoP_{i,m}} = \frac{\dot{e}_{i,m}}{\eta_{i.m}} \frac{\|T_i - T^*\|}{T^*} \tag{6}$$

Collecting terms after plugging (2), (3) and (4) into (5) and then substituting the result in (6), we obtain an expression for the individual non-discretionary demand for electricity for space conditioning, which is quadratic in the ambient outdoor temperature (given humidity) and linear in humidity (given temperature):

$$\begin{aligned} w_{i,m} = & \underbrace{\frac{\kappa_i^{\text{Conduction}}}{\eta_{i,m} T^*} \|T_i - T^*\| (T_i - T^*) \cdot \delta_m}_{\text{Conduction}} \\ & + \underbrace{\chi_{pa} \frac{\kappa_i^{\text{Convection}}}{\eta_{i,m} T^*} \|T_i - T^*\| (T_i - T^*) \cdot \delta_m}_{\text{Convection: Sensible Heat}} \end{aligned}$$

Figure 2: The Empirical Electricity Demand Response Function

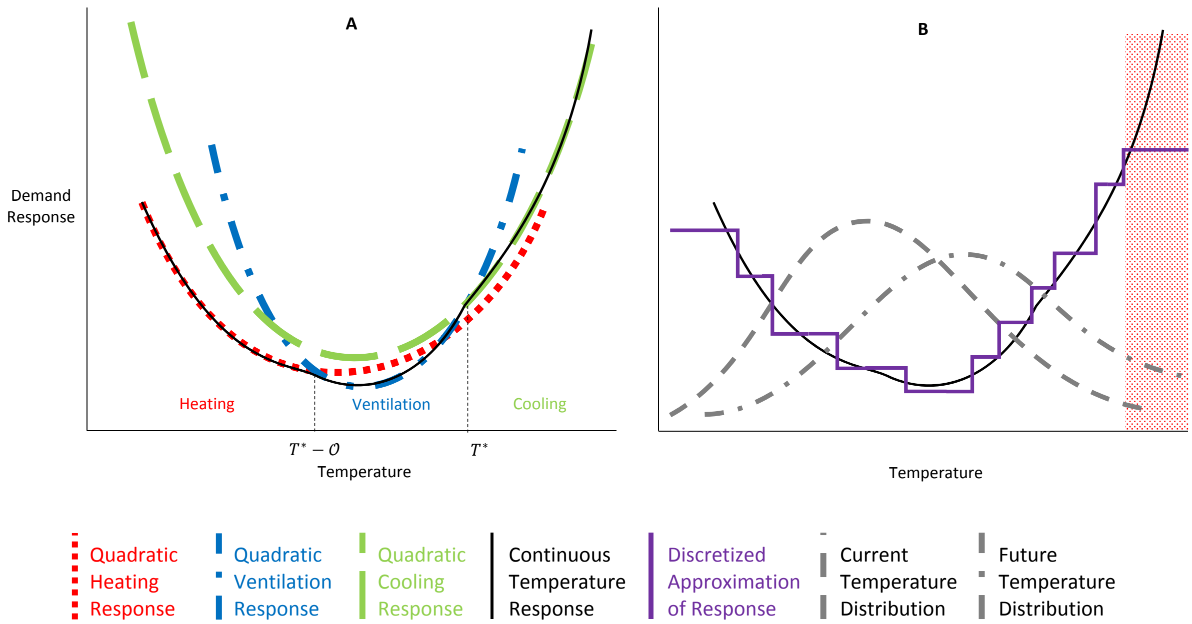

$$
\underbrace{+\frac{\kappa_i^{\text{Convection}}}{\eta_{i,m}T^*}\left\|T_i - T^*\right\|\left\{\chi_{ev}(H_i - H^*)\cdot\delta_m + \chi_{pv}(T_i\ H_i - T^* H^*)\cdot\delta_m\right\}}_{\text{Convection: Latent Heat}}
$$
$$
\underbrace{+\frac{\kappa_i^{\text{Radiation}}}{\eta_{i,m}T^*}\left\|T_i - T^*\right\|\Psi[x_i, y_i, t]\cdot\delta_m}_{\text{Radiation}}
$$
$$
\underbrace{+\frac{\iota}{\eta_{i,m}T^*}\left\|T_i - T^*\right\|\cdot\delta_m}_{\text{Internal Heat Gain}} \tag{7}
$$

where δ_m is an indicator function which takes the value -1 in heating mode, and 1 otherwise (cf eq. (5)).

Taking all modes together, the resulting electricity demand response function is a superposition of quadratic functions of temperature. Panel A of Figure 2 illustrates that the result is the black curve, which follows the U-shaped empirical profile estimated in the climate impacts literature (Aroonruengsawat and Auffhammer, 2011; Auffhammer and Aroonruengsawat, 2011; Deschenes and Greenstone, 2011). The most important way in which this model differs from prior studies is in the tails. The customary approach is a reduced-form semi-parametric regression of total electricity use over some averaging period (say a year or a month) on a discretized distribution of weather exposure made up of the frequency counts of shorter time units (days or hours) spent in discrete intervals or "bins" of temperature. For example, with b bins, the phenomenological analog of (7) is

$$w = \varpi + \sum_b \rho_b \, \mathcal{C}[T \in (\underline{T}_b, \overline{T}_b)] + \text{Controls} + u \tag{8}$$

where $(\underline{T}_b, \overline{T}_b)$ are the b^{th} interval's temperature boundaries, $\mathcal{C}$ denotes the counts of time periods where T falls into that interval, ϖ is a constant and u is a random disturbance term. The key assumption is that associated with each bin is a constant marginal effect, with the overall discretized response function given by the vector of estimated coefficients $\boldsymbol{\rho}$. This is illustrated in Figure 2 panel B as the stair-step curve, where each step's height indicates the demand impact of an additional day (say) of exposure in that particular temperature interval. While such an assumption may be innocuous over the bulk of the temperature probability distribution, it has the potential to introduce bias at the extreme bins, where our continuous model predicts that marginal effects are *increasing*. Indeed, the concern is that under climate change the distribution of temperature exposure will shift to the right, adding probability mass in the upper tail region where the marginal effects are least precisely estimated due to a paucity of historical observations.

3 Micro-Consistent Aggregation

Our second task is to consistently aggregate eq. (1) up to the level at which we observe electricity demand: the groups of counties that make up each ISO/RTO's weather zones, z. With linearity in the heterogeneous variables we can simply sum across individuals within zones:

$$\widetilde{Q}_z = \sum_{i \in z} q_i = \sum_{i \in z} (\gamma_i + w_i) + \frac{\sigma}{p_E} \left(\widetilde{\mathscr{I}_z} - p_E \sum_{i \in z} (\vartheta_i + w_i) - \sum_{g \neq E} p_g \widetilde{Y}_g \right) \tag{9}$$

where $\widetilde{Q}_z$, $\widetilde{\mathscr{I}_z}$ and $\widetilde{Y}_z$ are observed zonal aggregate electricity use, income, and consumption of other goods. Expressing (9) in per capita terms by dividing by zonal population (N_z) and rearranging yields:

$$Q_z = \widetilde{Q}_z / N_z = \Gamma_z + W_z + \sigma\left(\frac{\mathscr{I}_z}{p_E}\right) + \Upsilon_z\left(\frac{-1}{p_E}\right) \tag{10}$$

Obviously, this model is more applicable to residential electricity use than commercial and industrial demands, which are not separately observed. With the latter incorporated into the remaining terms, W is the price-invariant per capita expenditure on electricity for space conditioning, while Γ represents other non-weather related price-invariant per capita expenditure on other electricity. As a practical matter we can specify Γ as a time-dependent function as a way of capturing how the latter component of electricity use fluctuates with economic activity over days and weeks, and trends over years.

The problem of aggregating individual demands thus boils down to specifying W_z. The key impediment we face is that the parameters of (7) are heterogeneous and not observed by the econometrician, making direct summation of that expression impossible. Nevertheless, two characteristics of the problem can be exploited to come up with a solution. First, the parameters of (7) fundamentally depend on the attributes of the built environment, such as buildings' ratio of surface area to volume, the R-factor of their insulation, and the efficiency of their HVAC systems. Second, because local weather is determined by patterns of large-scale atmospheric circulation, at any instant of time large numbers of individuals over wide geographic areas will experience broadly similar ambient temperature and humidity exposures. This suggests that individuals in each zone can be grouped into $j \in J_z$ categories of buildings in each of $k \in K_z$ locations, giving rise to $j \times k$ archetypical patterns of HVAC electricity use:

$$\begin{aligned}
w^{\ddagger}_{j,k,m} = & \left\langle \frac{\kappa_j^{\text{Conduction}}}{\eta_{j,m} T^*} \right\rangle \{\|T_k - T^*\| \, (T_k - T^*) \cdot \delta_m\} \\
& + \left\langle \chi_{pa} \frac{\kappa_j^{\text{Convection}}}{\eta_{j,m} T^*} \right\rangle \{\|T_k - T^*\| \, (T_k - T^*) \cdot \delta_m\} \\
& + \left\langle \frac{\kappa_j^{\text{Convection}}}{\eta_{j,m} T^*} \right\rangle \{\|T_k - T^*\| \, \chi_{ev}(H_k - H^*) \cdot \delta_m + \chi_{pv}(T_k \; H_k - T^* H^*) \cdot \delta_m\} \\
& + \left\langle \frac{\kappa_j^{\text{Radiation}}}{\eta_{j,m} T^*} \right\rangle \{\|T_k - T^*\| \, \Psi[x_k, y_k, t] \cdot \delta_m\} \\
& + \left\langle \frac{\iota}{\eta_{j,m} T^*} \right\rangle \{\|T_k - T^*\| \cdot \delta_m\}
\end{aligned} \tag{11}$$

The implication is that with information on the distribution of population across locations and building types ($n^{\ddagger}_{j,k}$) per capita HVAC electricity use is easily calculated as the weighted sum

$$W_z = \sum_{j=1}^{J_z} \sum_{k=1}^{K_z} \sum_{m} \phi_{j,k} w^{\ddagger}_{j,k,m} \tag{12}$$

where the weights reflect the distribution of individuals by building type, $\phi_{j,k} = n^{\ddagger}_{j,k}/N_z$.

To take (12) to the data we substitute in eq. (11) and expand the result, collect like terms and rearrange the order of subscripts. Crucially, every term on the right-hand side of (11) is a product of components which are orthogonal in the j and k dimensions (the $j \times m$ heterogeneous unobserved coefficients in angle brackets and the $k \times m$ transformed weather observations in curly braces). Aggregating according to the inner product in (12) and collecting terms thus enables us to collapse (11) over the k spatial units, yielding $j \times m$ unknown parameters on each transformed meteorological covariate of similar dimension. The former are thermodynamic parameters, made up of complicated functions of the terms in angle brackets, T^* and H^*. The latter are the weighted averages of the terms in curly braces, stratified according to the temperature ranges that correspond to each mode. The result is a deceptively simple reduced-form quadratic function in temperature, humidity and insolation, with seven mode-specific parameters and a constant, given by the vector $\boldsymbol{\omega}$.

$$\begin{aligned}
W_z = \sum_{j=1}^{J_z} \Bigg[& \sum_m \omega^{T}_{j,m} \left(\sum_{k=1}^{K_z} \phi_{j,k} T_k \cdot \delta[T_k \in (\underline{T}_m, \overline{T}_m)] \right) + \sum_m \omega^{TT}_{j,m} \left(\sum_{k=1}^{K_z} \phi_{j,k} T_k^2 \cdot \delta[T_k \in (\underline{T}_m, \overline{T}_m)] \right) \\
& + \sum_m \omega^{TH}_{j,m} \left(\sum_{k=1}^{K_z} \phi_{j,k} T_k H_k \cdot \delta[T_k \in (\underline{T}_m, \overline{T}_m)] \right) + \sum_m \omega^{TTH}_{j,m} \left(\sum_{k=1}^{K_z} \phi_{j,k} T_k^2 H_k \cdot \delta[T_k \in (\underline{T}_m, \overline{T}_m)] \right) \\
& + \sum_m \omega^{\Psi}_{j,m} \left(\sum_{k=1}^{K_z} \phi_{j,k} \Psi_k \cdot \delta[T_k \in (\underline{T}_m, \overline{T}_m)] \right) + \sum_m \omega^{T\Psi}_{j,m} \left(\sum_{k=1}^{K_z} \phi_{j,k} T_k \Psi_k \cdot \delta[T_k \in (\underline{T}_m, \overline{T}_m)] \right) \\
& + \sum_m \omega^{H}_{j,m} \left(\sum_{k=1}^{K_z} \phi_{j,k} H_k \cdot \delta[T_k \in (\underline{T}_m, \overline{T}_m)] \right) \Bigg] + \omega^0_z
\end{aligned} \tag{13}$$

We further simplify this expression by assuming that each coefficient is made up of a systematic population-average component (β) and an idiosyncratic component that depends on the characteristics of each building type (ξ): $\omega_{j,m} = \beta_m + \xi_j$. Integrating out the idosyncratic components yields our final specification

$$\begin{aligned}
\mathrm{E}[W_z] = &\sum_m \beta_m^T \left(\sum_{k=1}^{K_z} \Phi_k T_k \cdot \delta[T_k \in (\underline{T}_m, \overline{T}_m)] \right) + \sum_m \beta_m^{TT} \left(\sum_{k=1}^{K_z} \Phi_k T_k^2 \cdot \delta[T_k \in (\underline{T}_m, \overline{T}_m)] \right) \\
&+ \sum_m \beta_m^{TH} \left(\sum_{k=1}^{K_z} \Phi_k T_k H_k \cdot \delta[T_k \in (\underline{T}_m, \overline{T}_m)] \right) + \sum_m \beta_m^{TTH} \left(\sum_{k=1}^{K_z} \Phi_k T_k^2 H_k \cdot \delta[T_k \in (\underline{T}_m, \overline{T}_m)] \right) \\
&+ \sum_m \beta_m^{\Psi} \left(\sum_{k=1}^{K_z} \Phi_k \Psi_k \cdot \delta[T_k \in (\underline{T}_m, \overline{T}_m)] \right) + \sum_m \beta_m^{T\Psi} \left(\sum_{k=1}^{K_z} \Phi_k T_k \Psi_k \cdot \delta[T_k \in (\underline{T}_m, \overline{T}_m)] \right) \\
&+ \sum_m \beta_m^{H} \left(\sum_{k=1}^{K_z} \Phi_k H_k \cdot \delta[T_k \in (\underline{T}_m, \overline{T}_m)] \right) + \beta_z^0 \qquad (14)
\end{aligned}$$

where the weights are simply the locations' population shares ($\Phi_k = \sum_j n^{\ddagger}_{j,k}/N_z$). For the sake of computational tractability we perform our stratification over fixed temperature intervals that we assume correspond to each mode, with $\underline{T}_H = \overline{T}_V = 64°\text{F}$, $\underline{T}_C = \overline{T}_V = 71°\text{F}$, $\underline{T}_H = -\infty$ and $\overline{T}_C = +\infty$, per (5).

4 Data and Estimation

4.1 Data

We amass an impressive quantity of data to perform our empirical analysis. Data on electricity use with the highest spatial and temporal resolution come from independent system operator (ISO) filings to the Federal Energy Regulatory Commission (FERC). ISOs are independent organizations which are responsible for the management, operation and control the electricity grid, administration of wholesale electricity markets, and provision of reliability planning for the bulk electricity system at the regional level. Because they must ensure that the supply of electricity equals demand on a millisecond basis, ISOs record and archive vast quantities of highly disaggregated data on electric power load, generation and transmission, and make this information publicly available in some form.

Table 1: Descriptive Statistics of ISO Load Data

Zone	Number of Counties	Annual Population (millions) %-tiles: 25th	50th	75th	Load (GWh) %-tiles: 25th	50th	75th
Electric Reliability Council of Texas (ERCOT) 4/16/2003 [13:00]-12/31/12 [23:00] (85,019 hours)							
Coast	12	5.330	5.772	6.044	8.517	9.584	11.480
East	20	0.992	1.035	1.063	1.224	1.422	1.712
Far West	22	0.396	0.417	0.429	1.061	1.168	1.333
North	27	0.494	0.496	0.497	0.784	0.906	1.082
North Central	33	6.674	7.153	7.420	9.714	11.171	13.723
South Central	25	3.591	3.942	4.129	4.707	5.455	6.688
Southern	26	2.075	2.185	2.265	2.328	2.730	3.328
West	29	0.548	0.558	0.568	0.845	0.953	1.120
New York ISO (NYISO) 1/1/2002 [0:00]-12/31/2012 [23:00]* (96,319 hours)							
Capitl	13	1.253	1.268	1.275	1.123	1.306	1.459
Centrl	16	1.611	1.613	1.619	1.673	1.899	2.094
Dunwod	1	0.933	0.936	0.951	0.576	0.691	0.785
Genese	7	1.168	1.171	1.176	0.976	1.149	1.274
Hud Vl	10	2.661	2.676	2.710	1.016	1.172	1.317
Mhk Vl	18	2.069	2.080	2.082	0.735	0.868	0.983
Millwd	1	0.933	0.936	0.951	0.235	0.295	0.357
NYC/LongIl*	7	10.860	10.868	10.879	6.975	8.382	9.348
North	5	0.289	0.290	0.290	0.625	0.711	0.763
West	11	2.461	2.463	2.483	1.612	1.823	2.011
ISO New England (ISO-NE) 3/1/2003 [0:00]-12/31/12 [23:00] (86,256 hours)							
CT	8	3.507	3.546	3.577	3.129	3.711	4.186
ME	16	1.319	1.328	1.329	1.134	1.343	1.467
NE Mass Bost	4	3.533	3.575	3.649	2.520	2.967	3.283
NH	10	1.298	1.316	1.317	1.108	1.348	1.496
RI	5	1.053	1.055	1.068	0.793	0.948	1.060
SE Mass	5	1.279	1.281	1.288	1.458	1.746	1.957
VT	14	0.621	0.624	0.626	0.591	0.694	0.764
WC Mass	5	1.602	1.613	1.626	1.765	2.082	2.321

* The NYC/LongIl series stops at 1/30/2005 (23:00) and only has 26,892 observations

For our dependent variable we use hourly load within sub-zones of service territories of the three ISOs in Figure 1. As summarized in Table 1, these three organizations archive over a decade's worth of load data at a fine level of spatial detail—aggregations of counties into "weather zones" that tend to experience similar hourly meteorological conditions.

We match these observations to a historical weather dataset—the North American Land Data Assimilation System (NLDAS-2) forcing files, which are ultimately derived from hourly measurements at thousands of weather stations throughout the U.S. These observations are used to constrain an atmospheric model which simulates atmospheric circulation and associated fluxes of heat, mass

Table 2: Descriptive Statistics of Weather and Economic Covariates

A. Weather Covariates

	ERCOT						NYISO						ISO-NE					
	Heating[a,d]		Ventilation[b,d]		Cooling[c,d]		Heating[a,d]		Ventilation[b,d]		Cooling[c,d]		Heating[a,d]		Ventilation[b,d]		Cooling[c,d]	
	Mean	S.D.	Mean	S.D.	Mean	S.D.	Mean	S.D.	Mean	S.D.	Mean	S.D.	Mean	S.D.	Mean	S.D.	Mean	S.D.
$T \times 10^{-1}$	28.18	0.492	29.3	0.068	30.29	0.418	27.73	0.776	29.31	0.1	29.89	0.227	27.79	0.752	29.31	0.081	29.92	0.206
$T^2 \times 10^{-2}$	794.6	27.56	858.6	3.964	917.6	25.44	769.7	42.83	859.3	5.88	893.5	13.58	772.6	41.57	859	4.736	895.4	12.36
$T \times H \times 10^{-2}$	13.9	6.61	33.35	8.523	42.17	10.26	13.2	7.363	34.8	6.053	44.25	7.18	13.59	7.54	36.26	5.6	44.74	7.085
$T^2 \times H \times 10^{-3}$	394.1	192.1	977.4	250	1277	307.9	371.3	215.6	1020	178.7	1324	220	382.9	220.4	1063	165	1339	215.8
$\Psi \times 10$	1.48	2.402	2.32	3.042	3.617	3.621	1.753	2.5	2.803	3.274	4.479	3.381	1.786	2.533	2.856	3.259	4.575	3.325
$T \times \Psi$	41.91	68.08	67.97	89.15	109.8	110	48.98	70.28	82.17	96.01	134	101.1	50.03	71.33	83.71	95.54	136.9	99.46
Share of hours (%)[d]	27.10		1.70		39.50		70.30		4.70		7.70		71.10		4.20		5.30	

[a] $T \leq 291\text{K}$ ($\approx 64°\text{F}$), [b] $291\text{K} < T < 295\text{K}$, [c] $295\text{K} \leq T$ ($\approx 72°\text{F}$)
[d] The shares do not sum to 100% because these summary statistics are generated from the subset of observations where all zones are completely within a given HVAC mode. The difference represents hourly observations where different counties in each zone are in different HVAC modes, which is common in the shoulder seasons in northerly locations.

B. Economic Covariates

	ERCOT			NYISO			ISO-NE		
	%-tile: 25th	50th	75th	%-tile: 25th	50th	75th	%-tile: 25th	50th	75th
Load per Capita (kWh/person)	1.348	1.645	2.133	0.466	0.776	1.095	0.863	1.036	1.223
Temperature (K)	287.4	295.2	300.9	274.1	282.8	291.2	274.7	283.1	290.8
Humidity (g H_2O/kg Air)	5.9	10.6	14.1	3.3	5.9	10.4	3.3	6.1	10.4
Residential Electricity Price* (¢/kWh)	9.1	10.1	11.1	14.9	16.2	16.9	13.2	14.2	15.7
Commercial Gas Price* ($/1000 ft^3)	4.44	6.40	7.78	8.16	9.25	11.78	9.54	11.73	13.93
Income per Capita* ($/month)	3,218	3,346	3,467	3,946	4,271	4,388	3,489	3,791	4,478
Income ÷ Electricity Price* (kWh/person)	30,023	32,380	35,301	24,674	26,153	27,470	25,120	26,565	28,729
Reciprocal of Electricity Price* (kWh/$)	8.976	9.947	10.972	5.917	6.171	6.700	6.370	7.054	7.567

* 2012 dollars, nominal values deflated using the CPI

and moisture at different altitudes above the land surface. These calculations generate continuous spatial fields of meteorological variables at the surface on a $1/8°$ raster grid at an hourly time-step over the coterminous U.S., accounting for the effects of topography (Mitchell et al, 2004; Xia et al, 2012). Like previous researchers, our principal focus is temperature, but we also investigate the role of humidity because the quantity of moisture in the air is a driver of comfort, and its latent heat can affect HVAC workloads. The raster grid differs from the geographies at which we observe electricity loads (zones) and building characteristics (counties), necessitating aggregation. Bilinear interpolation over cells in our raster fields up to the level of county polygons enables us to construct county-level hourly series of temperature and specific humidity.

Our insolation function is constructed based the central meridians of U.S. time zones and the dates of daylight saving time recorded by the US Naval Observatory. Temperature and incident solar energy flux are strongly correlated. The resulting pattern in Ψ is a daily sinusoid which is censored whenever the sun is below the horizon, peaks earlier in the eastern locations and later in the west, and exhibits higher peaks and longer periodicity during summer months and at more southerly locations (see Appendix Figure A.1). We also compute the interactions between temperature and insolation and humidity and insulation at each county centroid at each hour. Descriptive statistics for these variables are shown in Table 2, panel A. We operationalize (14) by approximating the weights Φ_ks using annual county-level population estimates from the Census Bureau, which we linearly interpolate down to our hourly time-step.

Turning to the economic covariates in (10), our proxy for electricity prices is monthly average revenue per kWh, which we calculate from EIA state-level monthly series of electricity sales and revenue to residential, commercial, and industrial customers. Although the resolution of these data is coarse in comparison to our dependent variable, the standard monthly electricity billing cycle suggests that most consumers are unlikely to respond to price signals on shorter time scales. Monthly price series should therefore be adequate controls for long-run demand responses. To control for potential simultaneity bias in using the electricity price to estimate demand, we also gathered data on candidate instruments: state-level monthly natural gas average revenue per 1000 ft^3 for industrial customers. Our reasoning is that increasing the wholesale price of natural gas will drive up the marginal cost of generation and the price of electricity, but will not directly affect electricity consumption for cooling in summer months because AC is powered exclusively by electricity. We also collected county-level annual per capita personal income from BEA. This variable directly enters into the residential demand function but in the present context proxies for the scale of overall economic activity. We linearly interpolate this series down to a monthly time-step using each year's monthly distribution of national personal income from the NIPAs. Finally, we deflate our nominal income and prices series to the 2012 base year using the monthly CPI from BLS. These data are summarized in Table 2, panel B.

Finally, to investigate the implications of our thermodynamic model, we collect gridded 3-hourly fields of future temperature and humidity simulated by global climate models (GCMs) under two different scenarios of warming from the Coupled Model Intercomparison Project version 5 (CMIP5— Taylor et al, 2012). The particular model we choose for this study is the Goddard Institute for Space Sciences GISS-E2-R (Miller et al, 2014; Schmidt et al, 2014), simulated under representative concentration pathways (RCPs) of radiative forcing which by the year 2100 rise to 4.5 W/m^2 (moderate warming, indicative of some effort to mitigate GHGs) and 8.5 W/m^2 (strong warming, a no-policy "business as usual" scenario). Hereafter we refer to these projections as RCP4.5 and RCP8.5 (for details, see Van Vuuren et al, 2011).

Descriptive statistics of our matched load and weather data in Figure 3 highlight the critical impact of temperature on peak power consumption. Panel A presents hourly load profiles for summer days shown, where demand peaks in the late afternoon and the height of the peak increases dramatically on days with high average temperatures, suggesting power consumption for AC. Although the relatively cool Northeast has a peak per capita consumption half that of Texas and exhibits a daytime hourly load profile that on cool days is nearly flat, the average per capita difference in the peak loads on warm and cool summer days is of comparable magnitude. Panel B presents these same data as a scatter plot along with a nonparametric lowess smooth load response to temperature. Color coding observations according to bins of daily temperature indicates the underlying relationship between average and instantaneous heat. Again, in the cooler Northeast the two are strongly correlated, but because a hot day in New England is equivalent to an average day in Texas,

Figure 3: Temperature Impacts on Summer Per Capita Load

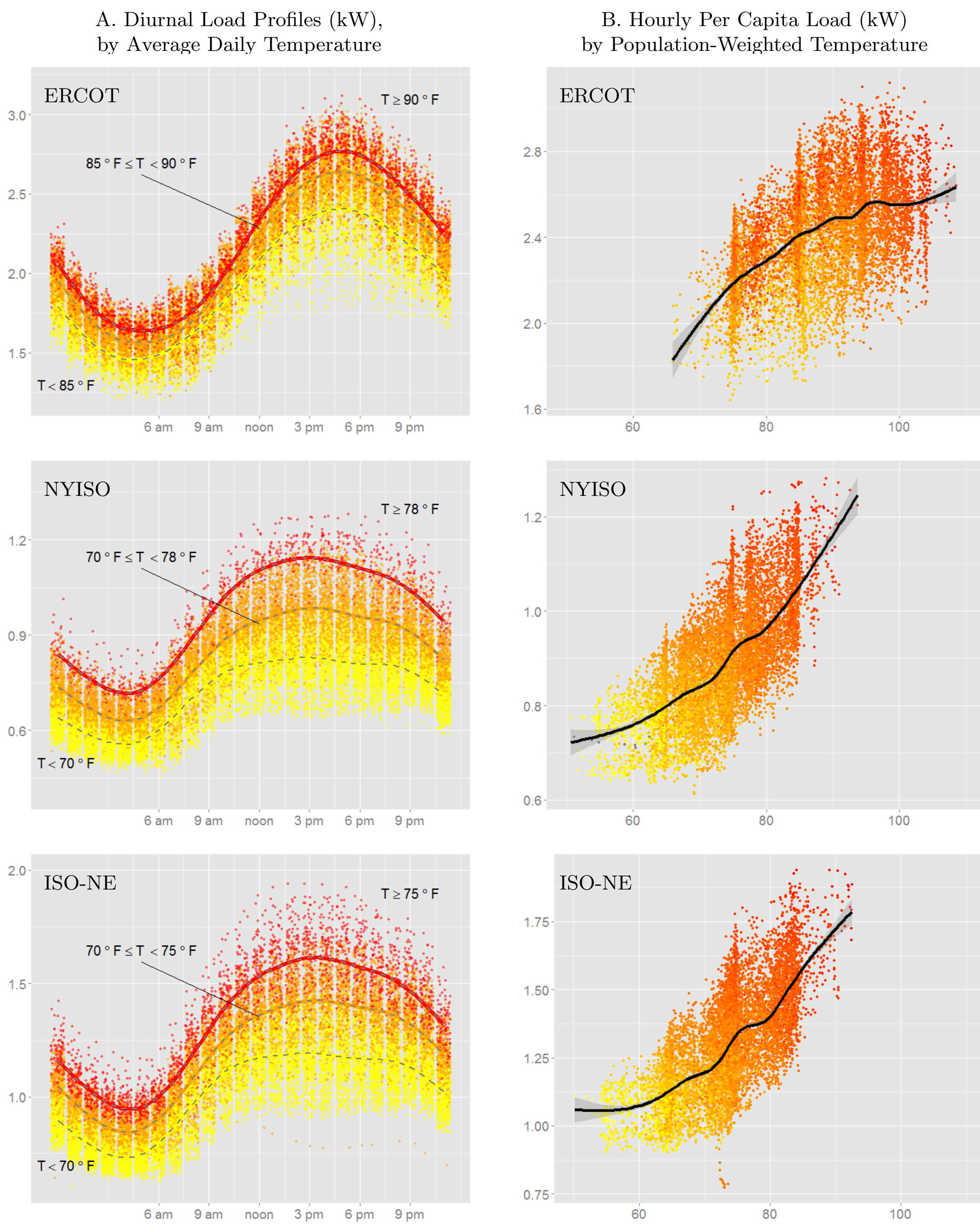

Figure 4: Relationship Between Maximum and Average Daily Temperatures (°F)

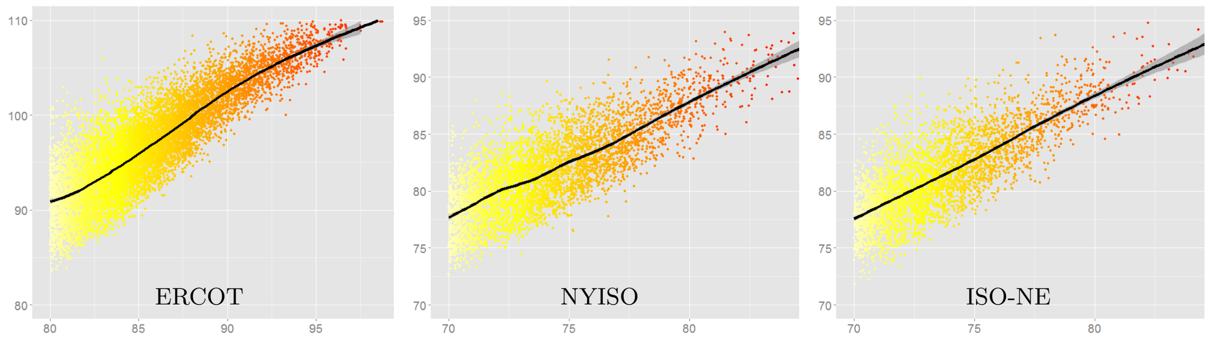

high peak temperatures are more evenly distributed across days whose average temperature can be as low as 75°F or as high as 95°F. Inspection of the smoothed response surfaces suggests that the average marginal effect of temperature in kW/person per °F is around 0.03 in Texas, 0.025 in New England and 0.016 in New York. However, in none of these regions is the marginal response constant—indeed, it appears to be increasing in the Northeast and declining in Texas. We are quick to emphasize that this may simply reflect underlying variation in other determinants of demand, particularly humidity.

Figure 3 suggests a simple back-of-the-envelope calculation to test the implications of estimates in the climate economics literature. Deschenes and Greenstone (2011) estimate than an additional day > 90°F will increase the log of annual energy consumption by 0.0037, equivalent to a 0.37% rise. In 2012, Texas's 26.06 million residents consumed 365,467 million kWh of electricity for an average per capita demand of 14,024 kWh, which suggests that one more day with such extreme heat will result in an additional 52 kWh/person of electricity consumption on average. Assuming that temperature and power consumption are contemporaneous, the equivalent average hourly increase is 2.34 kW/person, but this is an underestimate because the afternoon hours account for a disproportionate share of the daily total. Our average curve for a > 90°F day in the ERCOT region integrates to approximately 53 kWh/person, of which 8.25 kWh/person, or 16%, are in the peak 3 hours. The upshot is that in an average peak hour we can expect an additional $0.16 \times 52/3$ $= 2.8$ kW/person, which is just below the extremum of our observations.

One should be wary of taking comfort in such congruence, however. As Figure 4 drives home, a 90°F day is associated on average with a maximum daily temperature of around 103°F. Multiplying this value by our marginal effect from Figure 3 yields a peak demand of 3.09 kW/person, some 10% larger than the figure above. Even worse, the traditional approach lumps a 95°F day into the same interval as a 90°F day, and goes on to ascribe to it the same influence at the margin. The former is associated on average with a maximum daily temperature of around 107°F, for a peak demand of 3.2 kW/person, almost 15% larger.

4.2 Estimation

We assemble the data for all weather zones in each ISO and use the result to estimate (10) as a panel data regression with a rich set of fixed effects. Even though our structural parameters are generally not recoverable (e.g. we cannot separately identify thermal resistance from exposure area) identifying them is not necessary to address the question of how to make valid out-of-sample forecasts.[4] Every zone is assigned its own fixed effect (λ_z) to capture time-invariant idiosyncratic influences that are unrelated to whether such the intercept of the thermodynamic model which combines setpoint temperature/humidity and internal heat gain, as well as electricity demands by industry. We also include fixed effects for hour of day (HourOfDay) and day of week (DayOfWeek) to control for deterministic variation in economic activity demanding power (e.g., lower demand late at night or on weekends). Additionally, demand varies stochastically over longer time scales (e.g., over the course of the business cycle), which we account for by including year-month fixed effects (Year×Month). The latter absorb variation associated with not just business cycle phenomena, but, crucially, also the economic covariates recorded with at best monthly frequency. Hence, year-month dummies obviate the need to include prices and income in our estimating equation. While these economic parameters can of course be recovered from a second-stage regression of the estimated year-month effects on prices and income, they are tangential to our main research question. We therefore end up with a reduced form specification that is linear in the parameters and

[4]By contrast, investigation of counterfactual policy changes for climate adaptation, such as building efficiency improvements, can only be pursued by explicitly identifying these structural parameters, which in turn will require additional data to be brought to bear on the problem.

straightforward to estimate via OLS:

$$Q_{z,t} = \lambda_z + \text{HourOfDay}[t] + \text{DayOfWeek}[t] + \text{Year}\times\text{Month}[t] + \text{E}[W]_{z,t} + \varepsilon \tag{15}$$

By way of comparison we also classify temperature and humidity at each hour into bins, weight each bin according to the county populations in each weather zone, and use the resulting zonal series to estimate a semi-parametric panel regression that is the analog of (8):

$$\begin{aligned} Q_{z,t} = \lambda_z &+ \text{HourOfDay}[t] + \text{DayOfWeek}[t] + \text{Year}\times\text{Month}[t] \\ &+ \sum_b \theta_b^T \mathcal{N}[T_{z,t} \in (\underline{T}_b, \overline{T}_b)] + \sum_c \theta_c^H \mathcal{N}[H_{z,t} \in (\underline{H}_c, \overline{H}_c)] + v \end{aligned} \tag{16}$$

5 Results

5.1 Estimation Results

Our estimated coefficients are summarized in Table 3. The model is very precisely estimated, with both the continuous covariates and the fixed effects explaining over 85% of the variation in per capita load. Weather covariates are uniformly highly significant for cooling, and generally significant for other modes. Exceptions are temperature-humidity interactions in ventilation and New England's temperature impacts on electricity for both ventilation and heating (which is unsurprising given the widespread use of natural gas as a heating fuel). Figure 5 provides visualizations of our estimated responses. The temperature-demand relationships in panel A follow the U-shaped pattern in Figure 2. Texas exhibits the largest hourly non-weather related demand (1.75 kW/person) and a symmetric response to low and high temperatures, reflecting the prevalence of electric heating. Responses in the Northeast are asymmetric with AC responses that are strongly convex (per the discussion of heating fuel above), with significantly smaller non-weather related demands (1-1.2 kW/person). The results of the semiparametric model, superposed for comparison, follow a generally similar pattern to our smooth thermodynamic response. Even so, they tend to overestimate demand at moderate temperature intervals while underestimating demand in the extreme bin. Accounting

Table 3: Estimated Responses to Temperature, Humidity and Insolation by ISO/RTO

	ERCOT		NYISO		ISO-NE	
Heating						
T	-8019.0	(147.7)*	-1457.0	(22.7)*	-182.4	(23.6)
T^2	138.5	(2.6)*	25.8	(0.4)*	1.8	(0.4)
$T \times H$	-3797.0	(425.3)*	-4054.0	(73.0)*	-3136.0	(77.8)*
$T^2 \times H$	68.7	(7.4)*	70.7	(1.3)*	56.7	(1.4)*
Ψ	879.5	(11.1)*	113.4	(2.0)*	109.7	(2.2)*
$T \times \Psi$	-31.5	(0.4)*	-4.1	(0.1)*	-4.0	(0.1)*
H	52320.0	(6081.0)*	58160.0	(1048.0)*	43370.0	(1118.0)*
Ventilation						
T	-7800.0	(145.5)*	-1425.0	(30.1)*	-139.6	(31.1)
T^2	131.0	(2.7)*	24.6	(0.8)*	0.4	(0.8)
$T \times H$	-1624.0	(4277.0)	-4350.0	(1724.0)	253.9	(1863.0)
$T^2 \times H$	34.5	(72.9)	76.2	(29.3)	0.6	(31.7)
Ψ	621.5	(74.2)*	273.5	(28.2)*	347.8	(30.1)*
$T \times \Psi$	-22.6	(2.5)*	-9.7	(1.0)*	-12.3	(1.0)*
H	18040.0	(62750.0)	62120.0	(25340.0)	-7820.0	(27360.0)
Cooling						
T	-8207.0	(136.7)*	-1740.0	(22.0)*	-824.0	(23.1)*
T^2	144.8	(2.3)*	35.3	(0.4)*	23.5	(0.5)*
$T \times H$	3254.0	(130.7)*	-3533.0	(165.1)*	-6646.0	(200.9)*
$T^2 \times H$	-52.9	(2.2)*	58.0	(2.7)*	109.6	(3.3)*
Ψ	905.2	(7.4)*	288.3	(11.2)*	688.4	(13.1)*
$T \times \Psi$	-32.1	(0.2)*	-10.2	(0.4)*	-23.8	(0.4)*
H	-49820.0	(1972.0)*	53970.0	(2504.0)*	100900.0	(3044.0)*
Constant	11780.0	(2069)*	21460.0	(305.6)*	4579.0	(317.6)*
Adj. R-sq	0.85		0.95		0.91	
% of variation explained by:						
Weather covariates	0.50		0.07		0.24	
Fixed effects	0.73		0.93		0.84	
% of variation explained by Temperature and Humidity:						
Lower bound:	0.12		0.02		0.07	
Upper bound:	0.50		0.07		0.24	
N. Obs.	680,074		894,190		689,873	

for some of this divergence is the that the semiparametric model omits insolation and hence it is a confounder—temperature is absorbing the warming effects of insolation with which it is highly correlated. Hence, the model tends to overpredict demand at a given temperature changes because its marginal effects are actually picking up the joint effects of temperature and insolation.

The underlying temperature-humidity interactions are shown as response surfaces in panel B. The upper surface is the response of demand to temperature and humidity, holding all else constant. The lower surface is the kernel density of the observed hourly temperature and specific humidity over our sample. Each rendering is from a vantage point that provides the best view of both surfaces. The vertical axis of the lower surface is likelihood, which we have rescaled to facilitate interpretation. The density peaks at much lower temperatures in NYISO and ISONE than for ERCOT. That peak rises out of a ridge which traces our how the mode of specific humidity increases with temperature—the higher the temperature, the more energy is available for evaporation and the higher the atmospheric moisture concentration. The density dramatically falls beyond this ridge to zero along a convex curve in the temperature-humidity plane. The curve is the locus of saturation points at each temperature, below which moisture condenses out of the air in the form of precipitation. This saturation curve is a physical property, identical across ISOs, and the dispersion of the data around it indicates variation in local climate conditions.[5]

The upper surface is our estimated model. As in panel A, kW response is U-shaped in temperature but a straight line in humidity. Our fitted model produces an estimate of demand at every point in the temperature-humidity plane, but this can be misleading in regions which lie outside the envelope of observations. For instance, for $T > 90°$F specific humidity is rarely below 5g of water per kg of air—even in deserts; likewise, it is physically impossible for H to exceed the saturation point for the corresponding temperature. To present a slice of the 3D response surface which rules out such anomalies we do not simply hold specific humidity constant, instead we follow the curved ridge in the $T - H$ plane. In other words, we slice through the surface at the mean temperature for that humidity, which is equivalent to integrating out humidity using its marginal distribution at

[5] e.g., there is much more dispersion in ERCOT, reflecting Texas' wider range of climates (from dry desert in the west to humid subtropical coastal swamps in its east) compared to the mountain versus coastal climatic range of of New York and New England.

Figure 5: Estimated Temperature and Humidity Responses by ISO/RTO

A. Temperature

B. Temperature-Humidity Interactions

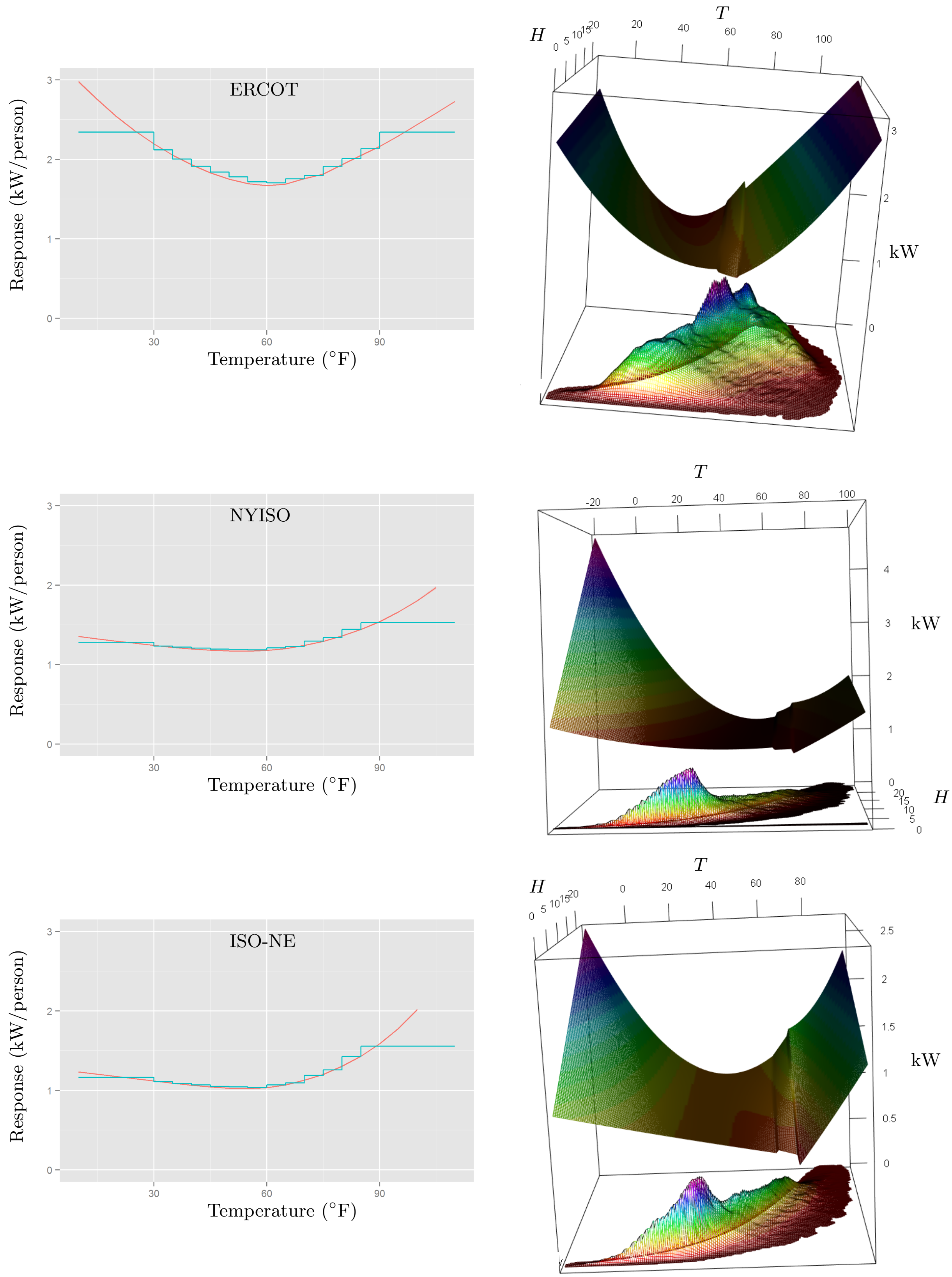

each temperature (or, as in much of the existing literature, simply ignoring humidity altogether). This explains why the splines in panel A show a much less dramatic response to cold extremes than warm extremes in New York and New England—here our slice through low temperatures occurs in the low-humidity region where the 3D surface is comparatively flat. We reiterate that this artifact of the data in no way vitiates our thermodynamic model—although increasingly cold ambient temperatures require the energy necessary to maintain comfort to increase in a convex fashion, northeast states fulfil such demand with gas, oil, and other non-electric energy sources.

5.2 Comparisons With Existing Reduced-Form Approaches

To quantify the implications of the divergence between thermodynamic and semiparametric regressions in the tails of temperature, we use our fitted models to generate synthetic hourly demands for each ISO's constituent counties over the period of our sample, from which we compute each county's backcasted annual peak demand and the corresponding temperature at that hour using the two methods. Our results, shown in Figure 6, illustrate the degree to which existing empirical approaches tend to underestimate the impacts of extreme temperatures. For the overwhelming majority of county-year annual peaks the semiparametric approach understates our thermodynamic model, with peaks at the highest temperature extremes observed in Texas biased downward by as much as 20%! As one might expect there is a closer correspondence between the two models in the cooler Northeast, but even though there is better agreement on the temperature at which peak load occurs, the semiparametric model still underestimates the magnitude of the peak by 5-10%.

5.3 Climate Change Implications

Our final set of results examines the implications of our thermodynamic model for response of peak and total electricity demand to climate change. Two challenges arise in forcing our fitted model with GCM projections. First, the highest temporal resolution at which the latter are available are 3-hour averages, which suggests that our forecasts will be biased downward relative to the true impact of warming on peak AC demand. Second, and more subtly, it is well known that

Figure 6: Semiparametric vs Thermodynamic Projections of Peak Electricity Consumption

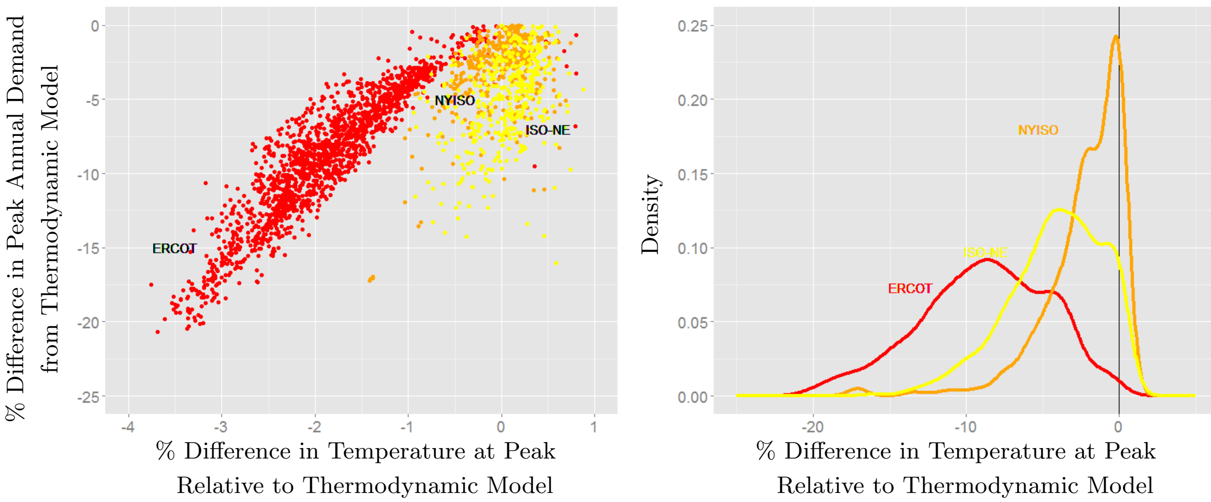

the internal variability of GCMs underestimates natural variability. This practical consequence is highlighted by Figure 7, which compares the likelihood of temperatures in different ranges. In Texas, the upper tail of the distribution of observed temperatures exceeds that of the distribution of future temperatures simulated by the GISS-E2-R GCM—*even with vigorous climate warming*. And while this phenomenon does not arise in the Northeast, the uppermost edge of the distribution of projected temperatures does not shift relative to the observational record.

For these reasons it is not appropriate to directly compare the results of our model forced by future climate change projections against the similar output forced by historical observations (as in our backcasting analysis)—especially of the results of such a comparison are sensitive to the tails of the distribution. Climatologists' solution to this problem is to "bias correct" the GCM output prior to its use for evaluating impacts (see, e.g., Christensen et al, 2008). While there are a plethora of approaches to bias correction, we use the simple approach of developing an apples-to-apples comparison by looking at the percentage changes in average peak load predicted by the GCM's gridded fields over the time-scale of decades. Specifically, we forecast annual peak and total electricity consumption for every year in the two epochs 2021-2050 and 2081-2100, compute the within epoch average at each county, and then calculate the percentage difference between the middle and the end of the 21st century

The results, shown in Figure 8, illustrate how the change in (integrated) total annual consump-

Figure 7: Density of Temperature: Observations (Green), RCP4.5 (Blue), RCP8.5 (Red)

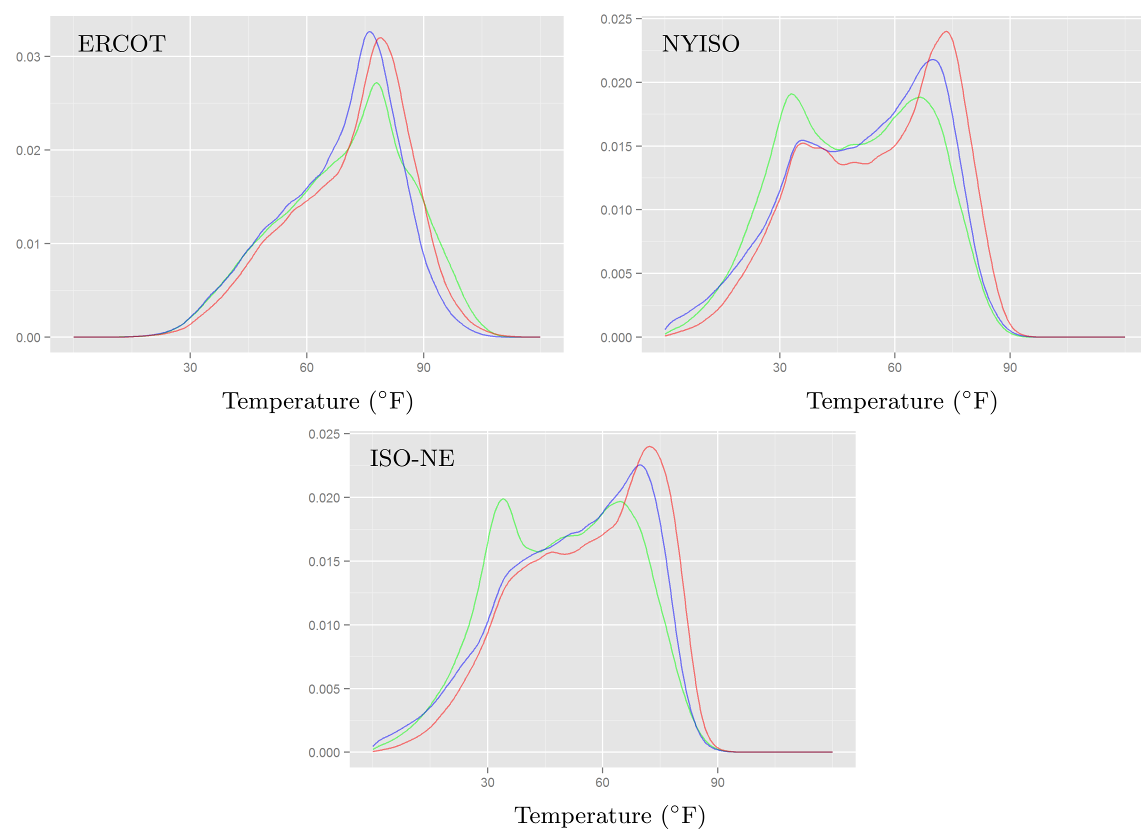

Figure 8: Climate Change Impacts on Total and Peak Electricity Consumption: 2081-2100 vs. 2021-2050

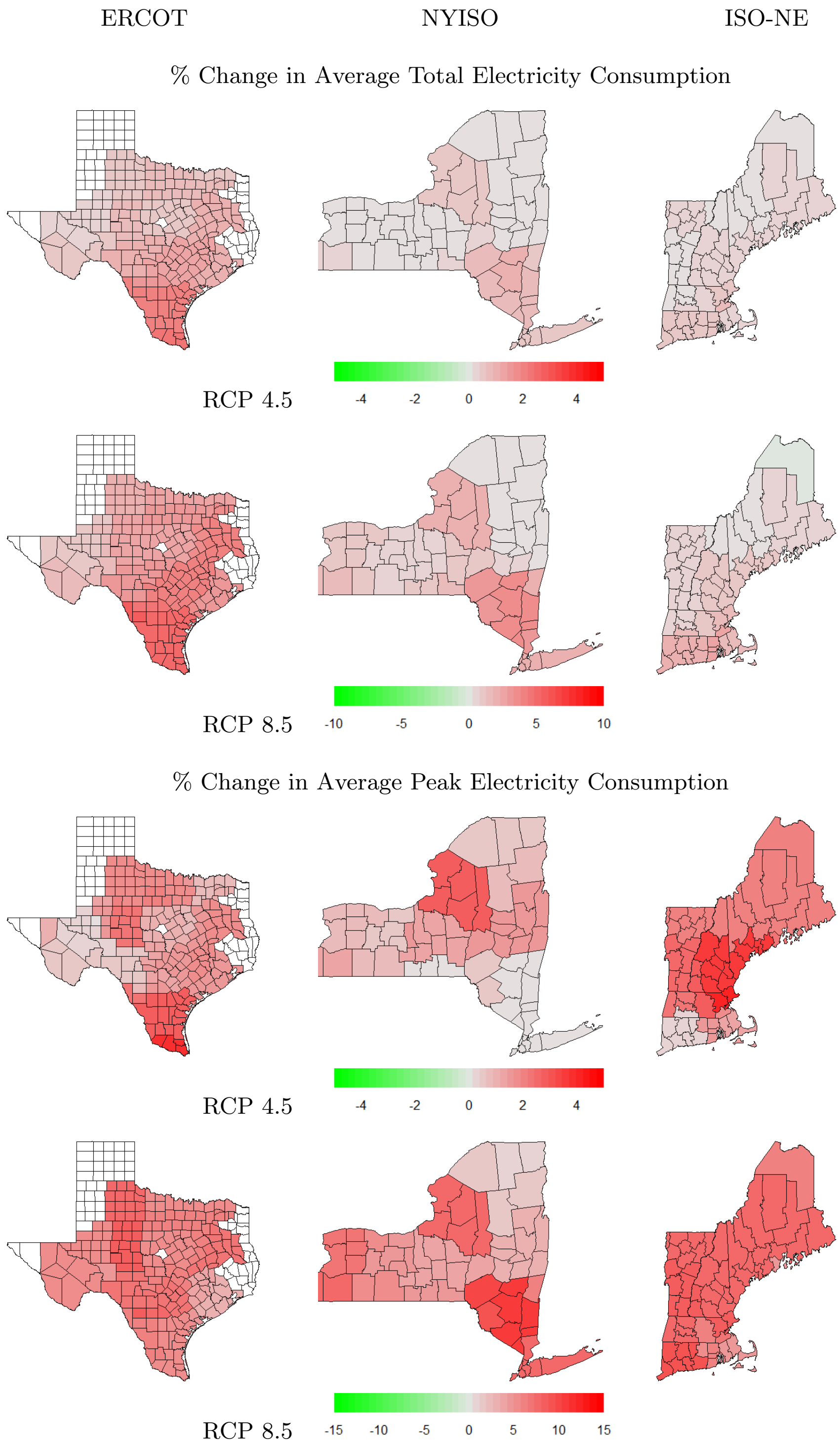

tion dramatically understates the (instantaneous) peak impact. As well, even though the former results might lead one to conclude that the impacts of climate change on electricity demand were comparatively modest in milder climates such as the Northeast, we show that the peak impacts are far more similar.

6 Conclusion

To be added.

Appendix

Our clear-sky approximation for insolation comes from the University of Oregon's Solar Radiation Monitoring Laboratory. Insolation depends on the daily distance from the Sun as Earth revolves along its asymmetric elliptical orbit, and the hourly zenith angle, α^{Zenith}, which describes the sun's deviation from directly overhead (when maximum insolation occurs). Our empirical impementation of the insolation function is

$$\Psi = (D_{\text{Avg}}/D_{\text{ES}})^2 \times \cos\alpha^{\text{Zenith}}[x_i, y_i, t_{\text{Clock}}, d] \times 1 \cdot \left(\cos\alpha^{\text{Zenith}}[x_i, y_i, t_{\text{Clock}}, d] > 0\right) \tag{A.1}$$

were D_{ES} is the Sun-Earth distance on a given day and D_{Avg} is the annual average distance. In this expression, the first term on the right-hand side is given by the polynomial

$$(D_{\text{Avg}}/D_{\text{ES}})^2 = 1.00011 + 0.034221\cos\nu + 0.001280\sin\nu + 0.000719\cos 2\nu + 0.000077\sin 2\nu \tag{A.2}$$

where ν is a function of the Julian date, $\nu = 2\pi(d/365)$. The second term, the zenith angle at $(x_i, y_i, t_i^{\text{Clock}})$, is given by the spherical law of cosines

$$\alpha_i^{\text{Zenith}} = \cos^{-1}(\sin\alpha^{\text{Dec}}\sin y_i + \cos\alpha^{\text{Hour}}\cos\alpha^{\text{Dec}}\cos x_i) \tag{A.3}$$

and depends on two parameters—the solar declination angle, α^{Dec} which is a function of Earth's axial tilt and orbital position on each Julian day, and the hour angle, α^{Hour} governing the movement of the sun across the sky. These are in turn given by

$$\alpha^{\text{Dec}} = \frac{23.45\pi}{180}\sin 2\pi\left(\frac{284+d}{365}\right) \tag{A.4}$$

$$\alpha^{\text{Hour}} = \pi(t^{\text{Solar}}/12 - 1) \tag{A.5}$$

where t_{Solar} denotes solar time, which is related to wall-clock time through a piecewise approximation

$$t^{\text{Solar}} - t_i^{\text{Clock}} + 1 \cdot \text{Daylight Saving[d]} - \frac{1}{15}(x_i^{\text{Std}} - x_i) = \begin{cases} -\frac{14.2}{60} \sin \pi \left(\frac{d+7}{111}\right) & d \in [1, 106] \\ \frac{4}{60} \sin \pi \left(\frac{d-106}{59}\right) & d \in [107, 166] \\ -\frac{6.5}{60} \sin \pi \left(\frac{d-166}{80}\right) & d \in [167, 246] \\ \frac{16.4}{60} \sin \pi \left(\frac{d-247}{113}\right) & d \in [246, 365] \end{cases} \tag{A.6}$$

where x_i^{Std} is the standard meridian of the time-zone in which a county resides (Eastern: 75°W, Central: 90°W, Mountain: 105°W, Pacific: 120°W). Daylight saving time is occasionally reset by Congress. The 1987 standard was the first Sunday in April until the last Sunday in October, and prevailed until the 2005 Energy Policy Act, which shifted the dates to the second Sunday in March until the first Sunday in November, effective 2007 (see `http://aa.usno.navy.mil/faq/docs/daylight_time.php`).

To evaluate the expression for Ψ we plug (A.4) and (A.5) into (A.3), then substitute the result along with (A.2) into (A.1). The resulting function is shown in Figure A.1 for the population-weighted centroids of counties in two weather zones: ISO New England's Maine and ERCOT's Far West (see Figure 1).

Figure A.1: Insolation in ISO-NE's Maine (ME) and ERCOT's Far West (FARWEST) Zones

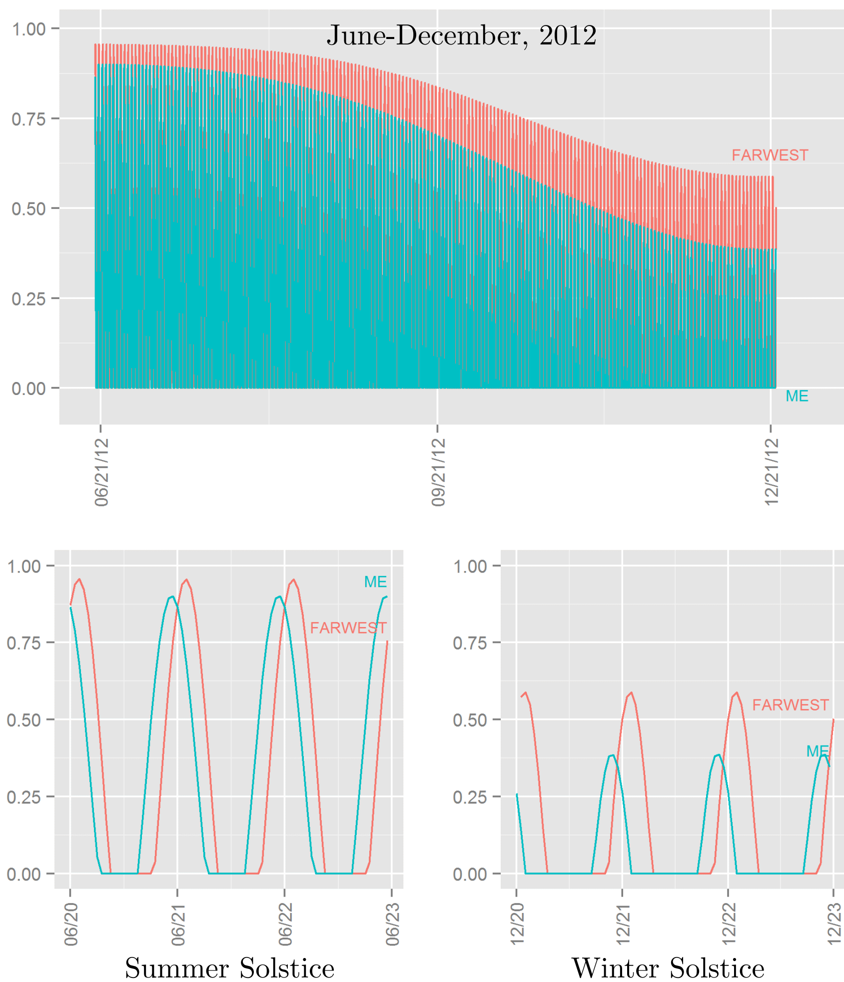

References

1. Allcott, H. (2013). Real-Time Pricing and Electricity Market Design, Working Paper, NYU Economics Dept.

2. Aroonruengsawat A, Auffhammer M (2011) Impacts of climate change on residential electricity consumption: evidence from billing data, in G. Libecap and R.H. Steckel (eds.), The economics of climate change: past and present. University of Chicago Press.

3. Auffhammer, M. and A. Aroonruengsawat (2011). Simulating the Impacts of Climate Change, Prices and Population on California's Residential Electricity Consumption. Climatic Change 109(S1): 191-210.

4. Christensen, J.H., F. Boberg, O.B. Christensen, and P. Lucas-Picher (2008). On the need for bias correction of regional climate change projections of temperature and precipitation, Geophysical Research Letters 35: L20709.

5. Dell, J., S. Tierney, G. Franco, R. G. Newell, R. Richels, J. Weyant, and T. J. Wilbanks (2014). Ch. 4: Energy Supply and Use. Climate Change Impacts in the United States: The Third National Climate Assessment, J. M. Melillo, Terese (T.C.) Richmond, and G. W. Yohe, Eds., U.S. Global Change Research Program, 113-129. doi:10.7930/J0BG2KWD

6. Dell, M., B.F. Jones, and B.A. Olken (2014). What Do We Learn from the Weather? The New Climate-Economy Literature, Journal of Economic Literature 52(3): 740-798.

7. Deschenes O., and M. Greenstone (2011). Climate Change, Mortality, and Adaptation: Evidence from Annual Fluctuations in Weather in the US, American Economic Journal: Applied Economics, 3(4): 152-85.

8. Herring, S. C., M. P. Hoerling, T. C. Peterson, and P. A. Stott, (eds.) (2014). Explaining Extreme Events of 2013 from a Climate Perspective. Bulletin of the American Meteorological Society 95(9): S1S96.

9. Izquierdo, M., A. Moreno-Rodrguez, A. Gonzlez-Gil, N. Garca-Hernando (2011). Air conditioning

in the region of Madrid, Spain: An approach to electricity consumption, economics and CO_2 emissions, Energy 36(3): 1630-1639.

10. Kharin, V.V., F.W. Zwiers, X. Zhang, and M. Wehner (2013). Changes in temperature and precipitation extremes in the CMIP5 ensemble, Climatic Change 119: 345-357.

11. Kodra, E. and A.R. Ganguly (2014). Asymmetry of projected increases in extreme temperature distributions, Scientific Reports 4: Art. no 5884 doi:10.1038/srep05884

12. Miller, R.L., G.A. Schmidt, L.S. Nazarenko, N. Tausnev, S.E. Bauer, A.D. Del Genio, M. Kelley, K.K. Lo, R. Ruedy, D.T. Shindell, I. Aleinov, M. Bauer, R. Bleck, V. Canuto, Y. Chen, Y. Cheng, T.L. Clune, G. Faluvegi, J.E. Hansen, R.J. Healy, N.Y. Kiang, D. Koch, A.A. Lacis, A.N. LeGrande, J. Lerner, S. Menon, V. Oinas, C. Perez Garca-Pando, J.P. Perlwitz, M.J. Puma, D. Rind, A. Romanou, G.L. Russell, Mki. Sato, S. Sun, K. Tsigaridis, N. Unger, A. Voulgarakis, M.-S. Yao, and J. Zhang, 2014: CMIP5 historical simulations (1850-2012) with GISS ModelE2, Journal of Advances in Modeling Earth Systems 6: 441-477.

13. Mitchell, K.E., D. Lohmann, P. Houser, E.F. Wood, J.S. Schaake, A. Robock, B.A. Cosgrove, J. Sheffield, Q. Duan, L. Luo, W.R. Higgins, R.T. Pinker, J.D. Tarpley, D.P. Lettenmaier, C.H. Marshall, J.K. Entin, M. Pan, W. Shi, V. Koren, J. Meng, B.H. Ramsay, and A.A. Bailey (2004). The multi-institution North American Land Data Assimilation System (NLDAS): Utilizing multiple GCIP products and partners in a continental distributed hydrological modeling system, Journal of Geophysical Research: Atmospheres 109 D7: 2156-2202.

14. Monitoring Analytics (2013). 2012 State of the Market Report for PJM, http://www.monitoringanalytics.com/reports/PJM_State_of_the_Market/2012/2012-som-pjm-volume1.pdf

15. Peterson, T. C. et al. (2013). Monitoring and understanding changes in heat waves, cold waves, floods and droughts in the United States: State of knowledge, Bulletin of the American Meteorological Society 94: 821-834.

16. Salamanca, F., M. Georgescu, A. Mahalov, M. Moustaoui, M. Wang and B.M. Svoma (2013).

Assessing summertime urban air conditioning consumption in a semiarid environment Environmental Research Letters 8: 034022 doi:10.1088/1748-9326/8/3/034022

17. Schmidt, G.A., M. Kelley, L. Nazarenko, R. Ruedy, G.L. Russell, I. Aleinov, M. Bauer, S.E. Bauer, M.K. Bhat, R. Bleck, V. Canuto, Y.-H. Chen, Y. Cheng, T.L. Clune, A. Del Genio, R. de Fainchtein, G. Faluvegi, J.E. Hansen, R.J. Healy, N.Y. Kiang, D. Koch, A.A. Lacis, A.N. LeGrande, J. Lerner, K.K. Lo, E.E. Matthews, S. Menon, R.L. Miller, V. Oinas, A.O. Oloso, J.P. Perlwitz, M.J. Puma, W.M. Putman, D. Rind, A. Romanou, Mki. Sato, D.T. Shindell, S. Sun, R.A. Syed, N. Tausnev, K. Tsigaridis, N. Unger, A. Voulgarakis, M.-S. Yao, and J. Zhang (2014). Configuration and assessment of the GISS ModelE2 contributions to the CMIP5 archive, Journal of Advances in Modeling Earth Systems 6: 141-184.

18. Taylor, K.E., R.J. Stouffer and G.A. Meehl (2012). An overview of CMIP5 and the experiment design, Bulletin of the American Meteorological Society 93(4): 485-498.

19. U.S. Energy Information Administration (2009). Residential Energy Consumption Survey, 2009, http://www.eia.gov/consumption/residential/index.cfm

20. 35. Van Vuuren, D.P., J. Edmonds, M. Kainuma, K. Riahi, A. Thomson, K. Hibbard, G.C. Hurtt, T. Kram, V. Krey, J.-F. Lamarque, T. Masui, M. Meinshausen, N. Nakicenovic, S.J. Smith and S.K. Rose (2011). The representative concentration pathways: an overview, Climatic Change 109: 5-31.

21. Xia, Y, K. Mitchell, M. Ek, J. Sheffield, B. Cosgrove, E. Wood, L. Luo, C. Alonge, H. Wei, J. Meng, B. Livneh, D. Lettenmaier, V. Koren, Q. Duan, K. Mo, Y. Fan and D. Mocko, (2012). Continental-scale water and energy flux analysis and validation for the North American Land Data Assimilation System project phase 2 (NLDAS-2): 1. Intercomparison and application of model products, Journal of Geophysical Research: Atmospheres 117 D3: 2156-2202.